AWARD NUMBER: W81XWH-13-1-0215

TITLE: Development of Magnetic Nanovectors for Treatment and Imaging of Breast Cancer Metastasis to the Brain

PRINCIPAL INVESTIGATOR: Omid Veiseh

CONTRACTING ORGANIZATION: Massachusetts Institute of Technology
Cambridge, MA 02139

REPORT DATE: October 2014

TYPE OF REPORT: Annual

PREPARED FOR: U.S. Army Medical Research and Materiel Command
Fort Detrick, Maryland 21702-5012

REPORT DOCUMENTATION PAGE

Form Approved
OMB No. 0704-0188

1. REPORT DATE	2. REPORT TYPE	3. DATES COVERED
October 2014	Annual	15 Sep 2013 - 14 Sep 2014

4. TITLE AND SUBTITLE

Development of Magnetic Nanovectors for Treatment and Imaging of Breast Cancer Metastasis to the Brain

5a. CONTRACT NUMBER

5b. GRANT NUMBER
W81XWH-13-1-0215

5c. PROGRAM ELEMENT NUMBER

6. AUTHOR(S)

Omid Veiseh

E-Mail:veiseho@mit.edu

5d. PROJECT NUMBER

5e. TASK NUMBER

5f. WORK UNIT NUMBER

7. PERFORMING ORGANIZATION NAME(S) AND ADDRESS(ES)

Massachusetts Institute of Technology
77 Massachusetts Avenue
Cambridge, MA 02139

8. PERFORMING ORGANIZATION REPORT NUMBER

9. SPONSORING / MONITORING AGENCY NAME(S) AND ADDRESS(ES)

U.S. Army Medical Research and Materiel Command
Fort Detrick, Maryland 21702-5012

10. SPONSOR/MONITOR'S ACRONYM(S)

11. SPONSOR/MONITOR'S REPORT NUMBER(S)

12. DISTRIBUTION / AVAILABILITY STATEMENT

Approved for Public Release; Distribution Unlimited

13. SUPPLEMENTARY NOTES

14. ABSTRACT

Treating breast cancer that has metastasized to the central nervous system remains a formidable challenge due to, 1) its high malignancy, 2) the difficulty in differentiating between tumor and healthy brain tissue, 3) the sensitivity of normal brain tissue to the toxicities of current therapies, 4) intrinsic cellular resistance of BMBC cells to chemotherapeutic drugs, and 5) the blood-brain barrier's (BBB) ability to prevent the passage of extrinsic substances such as drugs and contrast agents. Our aim is to develop magnetic contrast agents and targeted siRNA therapies capable of overcoming the blood brain barrier and to aid in both the diagnosis and treatment brain metastatic breast cancer. Magnetic nanoparticles with high susceptibility have been developed. These nanoparticles have been characterized to be monodispersed are working to engineer a nanovector that will aid in addressing the major challenges associated with the diagnosis and treatment of BMBC. The major components of the nanovector include a Fe3O4 superparamagnetic nanoparticle (NP) core and a shell comprised of a copolymer of polyethylene glycol (PEG)-grafted chitosan (C)-polyethyleneimine (P), or CP. The tumor targeting peptide, chlorotoxin (CTX), and siRNA (designed to knockdown the pro metastasis gene MENA) also are conjugated to the NP polymer overcoat.

15. SUBJECT TERMS
Nanotechnology, Targeted Therapies, RNAi

16. SECURITY CLASSIFICATION OF:			17. LIMITATION OF ABSTRACT	18. NUMBER OF PAGES	19a. NAME OF RESPONSIBLE PERSON
a. REPORT	b. ABSTRACT	c. THIS PAGE			USAMRMC
Unclassified	Unclassified	Unclassified	Unclassified	24	19b. TELEPHONE NUMBER *(include area code)*

Standard Form 298 (Rev. 8-98)
Prescribed by ANSI Std. Z39.18

Table of Contents

Page

Introduction

The aim of this research project is to develop a new generation of nucleic acid-carrier nanovectors that can pass biological barriers and non-invasively diagnosis, stage, treat and treat brain metastatic breast cancer. Despite advances made in breast cancer diagnosis and therapy, the prognosis for patients with brain metastasis remains dismal. Currently, only 20% of patients with breast cancer that has metastasized to the brain survive more than a year, and the incidence of this disease appears to be rising (*1, 2*). Treating breast cancer that has metastasized to the central nervous system (CNS) remains a formidable challenge due to: 1) its high malignancy, 2) the difficulty in differentiating between tumor and healthy brain tissue, 3) the sensitivity of normal brain tissue to the toxicities of current therapies, 4) intrinsic cellular resistance of metastasized breast cancer cells to chemotherapeutic drugs, and 5) the blood brain barrier's (BBB) ability to prevent the passage of extrinsic substances such as drugs and contrast agents (*3-5*). Use of superparamagnetic nanoparticles conjugated with targeting or therapeutic agents, combined with magnetic resonance imaging (MRI), has been recognized as a potential approach for early breast cancer detection and treatment. In this first year of this project we have focused on developing a nanovector that can address these challenges in the diagnosis and treatment of brain metastatic breast cancer. The major components of this nanovector include a Fe_3O_4 nanoparticle (NP) core and a shell comprised of a copolymer of polyethylene glycol (PEG)-grafted chitosan (C)-polyethyleneimine (PEI), or C-PEG-PEI. The tumor targeting peptide, chlorotoxin (CTX), and siRNA against the protein Mena is conjugated to the polymer overcoat of the NP. Mena is a protein which is recognized as member of the Ena/VASP family proteins that function to regulate cell motility through actin polymerization (*6*) (*7*) (*8*). Mena is shown to be upregulated in breast cancer cells and is a key mediator of cell metastasis (*6*). In this naovector system, the combination of chitosan and PEG form a biocompatible coating on the iron oxide core, stabilizing the strructure from agglomeration. The PEI protects siRNA from degradation by nucleases and facilitates proper intracellular trafficking of nanovector by promoting "endosomal escape". CTX (36-amino acids) is chosen because of its strong selective affinity for metastatic breast cancer cells. Upon completion of this project an optimized nanovector, detectable by MRI, and capable of effectively delivering siRNA to target MB cells to down regulate (or block) Mena gene expression down to therapeutically viable levels will be developed.

Body

Keywords: siRNA, Nanoparticle, Chlorotoxin, MENA protein, Brain Metastasis, MRI, and Blood Brain Barrier, Breast Cancer

OVERALL PROJECT SUMMARY

Aim1. Development of a magnetic nanovector (NPCP-siRNA-CTX) loaded with the therapeutic siRNA sequences designed to knockdown STAT3 expression, and monitoring of potency for killing Brain Metastasizing Breast Caner (BMBC) tumor cells in vitro (Months 1-24).

The MRI detectable nanovector system we aim to develop is comprised of a superparamagnetic iron oxide nanoparticle core (NP) and a shell of a biodegradable polymer PEG-grafted chitosan (CP), which is then subsequently modified with PEI to promote endosomal escape, siRNA designed to silence pro metastatic genes, and CTX, a peptide that specifically binds breast cancer (*9*). The CTX is a peptide that has been shown to effectively target metastatic tumor cells, and promote nanoparticle permeability across the BBB (*10*) through interaction with Annexin A2 receptors upregulated on endothelial cells of the neovasculature (*11*). We have termed this fully assembled nanovector system NPCP-siRNA-CTX.

Task1 a. Obtain and verify siRNA sequence that can knockdown (luciferase reporter gene, and pro metastatic gene of interest), in breast cancer cell lines (Time line for completion provided in SOW, Months 1-4)

During this year 1 reporting period (Months 1-4) we devoted significant effort towards the development of siRNA sequences that can be grafted on to our base chitosan-g-PEG coated iron oxide nanoparticle system. We specifically, have been able to foster a productive relationship with AXOlabs (Kulmbach, Germany), a world leader in the manufacturing of potent and robust oligonucleotides to provide us with siRNA oligos that we can graft onto our nanoparticles. Through discussions with there scientists we developed siRNA sequences that are specific for silencing the following reporter genes GFP and Luc. We also worked with their scientists to develop potent pan species siRNA sequence that can silence AHA1, house-keeping gene expressed by all cells in mice (Figure 1) so that we could better monitor potential off target effects in healthy tissue compared to specific silencing in cancer cells. Finally, for our therapeutic gene of interest MENA and its invasive isoform MENA-INV we synthesized and screened 6 different sequences of siRNA in order to identify one sequence that was effective at silencing both.

<u>Development of siRNA for covalent attachment</u>

To accomplish the covalent attachment chemistry we commercially procured siRNA designed to knockdown luciferase, GFP expression, or house keeping gene AHA1. For reporter sequences we contracted out AXO labs who aided us to screen a number of sequences and finally provided to us optimized sequences which These siRNA molecules where prepared with 5'thiol modification on sense strands and (fluorophore) modification on the antisense strand. The thiol modification was used to create a covalent linkage to the nanoparticle coating, and the

fluorphore provided a means for monitoring of siRNA delivery to brain tumor cells. Using a commercial transfection reagents such lipofectamine RNAi MAX (Life Technologies, Carlsbad, CA) we evaluated a number siRNA sequences and identified the sequence below to be most effective in down regulating the expression of GFP and Luc in breast cancer cells (4T1-GFP-Luc, and MDA-MB231-GFP-Luc).

siRNA sequences (against genes of interest) have been obtained from AXOlabs. AXOlabs has devised produces siRNA sequences using proprietary technology enables production of siRNA that is carefully designed to minimize off-target potential and off-target microRNA type potential (*12*). siRNA have been synthesized and evaluate to ensure high potency (IC50 in vitro in the range 1-100(500) pM) in order to prevent saturation of RISC complex when dosing effective quantities of siRNA. Chemical modifications have been introduced to stabilize siRNA for future *in vivo* applications, and reduce off-target potential of sense strand and minimize immune response.

GFP siRNA sequence-
5' Fluorophore (Cy5 or Cy5.5.)- 5'-AAGUCGUGCUGCUUCAUGUdTdT-3'-
Alexa647 Antisense Strand.
5' Th (Thiol, or DBCO)- 5'-AcAuGAAGcAGcACGACuUdT
sdT-3',– Sense Strand.
Based on qRT PCR analysis we determined that this sequence was effective in down regulating GFP expression >90%.

Luc siRNA sequence-
siLuc sense: 5' Fluorophore (Cy5 or Cy5.5.)- 5'-CUUACGCUGAGUACUUCGATT-3',
antisense: 5' Th (Thiol, or DBCO)- 5'-UCGAAGUACUCAGCGUAAGTT-3

Based on qRT PCR analysis we determined that this sequence was effective in down regulating GFP expression >90%.

Similarly, we evaluated the potency and specificity of siRNA sequences designed against AHA1
AHA1 siRNA sequence:
Antisense:5' Fluorophore (Cy5 or Cy5.5.) 5'-dAsCfuAfaUfcUfcCfaCfuUfcAfuCfcdTsdT-3'
Sense: 5'-(DBCO or Thiol)C6)-GfgAfuGfaAfgUfgGfaGfaUfuAfgUf(invdT)-3'

Based on qRT PCR analysis we determined that this sequence was effective in down regulating GFP expression >90%.

We also synthesized and screened 6 different sequences of siRNA designed to silence MENA and its invasive isoform MENA-INV. These sequences where designed with the goal of identifying a single sequence that is able to silence both MENA and MENA-INV. For screening of silencing we used MDA-MB231 that where transfected to overexpress MENA or MDA-MB231-MENA INV. For this experiment 6 different siRNA sequences where designed and synthesized (Table 1). These 6 sequences where then screened in vitro and evaluated using

qPCR for relative silencing of gene expression. Our results indicate siRNA sequence 6 to be the most efficacious at silencing both MENA and MENA-INV (Figure 2).

Task 1b. Synthesize NPCP-siRNA-CTX and validate tumor specificity *in vitro* (Months 1-12).

Synthesis of NPCP-siRNA-CTX nanovectors

We developed a conjugation scheme for the synthesis of NPCP-siRNA-CTX (Figure 3). As illustrated the process includes four major steps, 1) CP copolymer coupling, 2) nanoparticle synthesis and subsequent modification with PEI, 3) Functionalization with CTX, and 4) incorporation of siRNA onto nanoparticle. In the development phase parameters such as nanoparticle core/hydrodynamic size, zeta potential, density of coating, and the quantity of siRNA / CTX incorporated, have each be evaluated and optimized as needed in order to improve the overall functionality of the nanovector.

To increase the water solubility of chitosan and improve the anti-fouling properties of the coating material, we synthesized chitosan-grafted-PEG (CP) copolymer by conjugating mPEG to the amine groups of chitosan. However, since one end of the mPEG molecule ends with methoxy group and the other end has a hydroxyl group, its activation is necessary before conjugation and formation of the copolymer. Therefore, hydroxyl groups of the mPEG were first oxidized in the presence of acetic anhydride and DMSO to PEG-aldehyde.

Cation exchange chromatography was then used to remove unreacted PEG molecules purify a fraction of mono-PEGylated chitosan. The resulted fractions from each step were collected and their PEG percentages were determined using the UV spectroscopy method. The quantifications showed that the range of 0.5 to 1.2M NaCl (step II) corresponds to mono-PEGylated chitosan copolymer with homogeneous composition and molecular structure. The fraction collected at steps I had PEG ratios considerably more than one and the other fraction (step III) has almost no PEG.

To verify the successful attachment of PEG to chitosan, we used 1H NMR analysis to confirm the presence of bonded PEG after purifications. NMR samples were prepared by dissolving lyophilized CP powder in 5% solution of DCl in D2O (Figure 4 a). the specific peaks of the mPEG can be seen at 3.6 and 3.9ppm, which corresponds to methyl groups and ether bonds of the PEG. Furthermore, after conjugation, the H-1 and H-2 proton signals from chitosan shifted from 4.9 to 5.1 and from 3.2 to 3.4 ppm, respectively. These shifts correspond to the N-alkylation of chitosan after the reaction. The peak at 2.3 ppm is from the acetyl groups present in the structure of the chitosan. Other peaks of the saccharine backbone of chitosan were not well separated in the range of 3.6-4.5ppm, which is due to the overlapping of a more intense PEG peak. The peak at 4.7 ppm is also related to the D2O solvent used during the analysis. These results showed that PEG was covalently attached to the backbone of chitosan.

FTIR spectroscopy was additionally used to evaluate the molecular structure of CP copolymer (Fig. 4 b). The purified copolymer was lyophilized and analyzed after mixing with KBr at 1:100 weight ratios. The peak around 3400cm-1 corresponds to the OH stretching vibration band due to water molecules physically adsorbed to the polymer. The most characteristic peak of the chitosan is the absorbance band at 1000-1150 cm-1, corresponding to the deforming vibrations

of –C–O–C– groups. The band absorbance at 1655 cm-1 is reported to be related to carbonyl of amide groups (C=O), and the bands at 1560 and 1590 cm-1 are corresponded to the primary and secondary amine groups. The observed characteristic peaks of the PEG block of the copolymer can be also listed as: vas(CH2) at 2910cm−1, vs(CH2) at 2853cm−1, δ(CH2) at 1445cm−1, T(CH2) at 1350 cm−1, ω(CH2) at 1282cm−1, v(C–O) at 1241cm−1 and ω(–CH) at 947 cm−1. Peaks related to the aldehyde groups (v (C=O) at 1695cm−1) were not found in the spectra of copolymer, showing all the aldehyde groups were bonded to chitosan. In conclusion, FTIR spectra were consistent with NMR spectra and suggesting the successful conjugation of PEG to chitosan.

NPCP was produced by the co-precipitation of Fe^{2+} and Fe^{3+} ions in the presence of the mono-PEGylated copolymer. Polymer and iron ions solutions were mixed together at 40ºC and then ammonium hydroxide solution was added to this vigorously stirring mixture under inert conditions. The schematic illustrated in figure 3 outlines the key steps for the synthesis of NPCP. The first step of the synthesis reaction is preparation of a homogeneous polymer and iron ions solution. In this solution iron ions will complex with chitosan polymers through chelation interactions. Next, ammonium hydroxide is titrated in the solution and as the solutions pH is increased NP cores form in spatially confined copolymer matrix. In this reaction scheme the copolymer serves as a surfactant on the surface of the NPs to control the overall morphology, size and polydispersity of the produced NP's(*13*).

The thickness and density of the coating polymer plays an integral role on hydrodynamic size of produced NP's. To determine the optimal amount of surface coating molecules, four copolymer to iron molar ratios of 0.115, 0.172, 0.220 and 0.270 were used for in-situ synthesis and coating of the nanoparticles. A modified fluorescamine-based quantification methods was then used to determine the average number of the chitosan molecules on each individual nanoparticle. The number of the chitosan molecules is the same as the number of PEG molecules, since a mono-PEGylated copolymer was used as the coating. Fig. 5a shows that the average number of coating molecules increased 12-folds, when the polymer to iron molar ratio increased for only 2.5-folds. This result shows the higher efficiency of the coating reaction at higher ratios of the polymer, due to increased probability of the polymer-surface interaction at higher polymer concentrations. However, DLS measurements showed that the hydrodynamic size (Z-average) and PDI of the nanoparticles were very similar, distributed in narrow ranges of 35-45nm and 0.183-0.203 (Fig. 5b). Zeta potential measurement showed that the surface charges of the nanoparticles were in the neutral range (Fig. 5c).

Nanoparticles developed for biomedical applications should remain stable the biologically relevant solutions such as buffers and cell culture media. Here, 100µg of the NPCP prepared with varying degree of PEG molecules per NP were dispersed and incubated in 1 mL of Dulbecco's modified Eagle's medium (DMEM) with 10% of fetal bovine serum (FBS), Dulbecco's phosphate-buffered saline (PBS), and sodium bicarbonate buffer. The hydrodynamic size of the nanoparticles was measured with DLS method and the nanoparticles were considered unstable when their size grew to more than 250nm. The long-term stability of the nanoparticles in different biological media is shown in Figure 6. When there are about 353 PEG molecules on each NP, no significant change in hydrodynamic size was observed for at least 2 weeks in all the media. With increasing the amount of the copolymer from 28 to 353 molecules

per NP, the size of the NPCPs increased at least 3 to 5-folds in PBS and cell culture media and about 2 to 3 times in sodium bicarbonate solution. The stability improved when there were more protective PEG molecules on the surface of the nanoparticles.

The morphology and crystallographic structure of the iron oxide core determines its physical properties and surface characteristics. The nanoparticles where analyzed for morphology using HRTEM characterizations (Figure 7). Samples were prepared by depositing and vacuum drying of a drop of the diluted nanoparticle suspension on carbon coated copper grids (300 mesh). The general morphology and size distribution of the iron oxide core of the nanoparticles is shown in Figure 7a. The nanoparticles have a very well defined size distribution in the range of 5-8 nm. HRTEM analysis (Figure 7b), shows the constructive interference of the diffracted beams related to the (311) family planes with inter-planar distance of 0.25 Å, confirming the crystalline nature of the iron oxide nanoparticles. Selected Area Electron Diffraction (SAED) pattern of nanoparticles (Fig. 7c) showed bright and sharp spots, arranged as individual rings correlated to the (200), (220), (311) and (400) family planes of the magnetite, respectively from inner rings to the further ones. The bright and clear dot pattern of the rings proves that the nanoparticles have a high degree of crystallinity. This suggests that the strong bonding between the polymer and surface of the nuclei does not limit the growth of the NPs and iron ions can effectively diffuse through the polymer interface to attach to the atomic ledges available on the surface of the oxide core.

Integration of CTX and siRNA onto nanovector

We investigated a number of strategies for a covalent immobilization biomolecules siRNA, and CTX on to our nanoparticles. From our evaluations it is apparent that nanovectors synthesized through a covalent coupling scheme is significantly more stable and effective for targeting breast cancer cells. We synthesized a nanovector comprised of our base iron oxide nanoparticle coated with shell of Chitosan-g-PEG, which was subsequently modified with siRNA, and CTX both through covalent linkages. Post synthesis nanoparticles were modified with CTX and then siRNA was reacted to NP using the hetrobifunctional linker molecule m-Maleimidobenzoyl N-hydroxysuccinimide (MBS-1). MBS-1 carries an NHS portion that reacts with primary amines of chitosan on nanoparticle shell, and a maleimide moiety, which reacts with thiol groups of siRNA. The MBS-1 molecule is first reacted with NP-CTX at a 10,000 fold excess of MBS-1 molecules per NP in PBS/5mMM EDTA buffer pH 7.4 for 30 min. NP's are then rapidly purified through gel permeation chromatography to remove excess MBS-1 molecules. The thiol modified siRNA molecules are then mixed with MBS modified NP's at NP:siRNA (w:w) ratio of 10 and allowed to react for 1 hour. Using gel electrophoresis we where able to confirm the attachment of CTX (Figure 8) and siRNA (Figure 9) onto NPCP.

Characterization of preferential uptake of NPCP-siRNA-CTX by MMP2 expressing cells compared to non-MMP2 expressing control cells.

The targeting specificity NP-siRNA conjugated with CTX was optimized and confirmed in vitro using breast cancer tumor cells. The preferential uptake of NP-CTX-siRNA nanovectors by MMP2 expressing cells was compared to control non-MMP2 expressing cells conjugates over a range of treatment doses. In these studies the fluorescence properties of siRNA was monitored

using flow cytomtery to determine the relative internalization of siRNA through targeting. Cells where treated for 1.5 hours and then evaluated for mean fluorescence intensity using a Facs Canto (Benton Dickinson, Franklin Lakes, NJ) flow cytometer. As shown in Figure 10 preferential internalization by the MMP2 expressing cells of siRNA was demonstrated through targeting with CTX modified nanovector.

Task 1c. Synthesize and validate NPCP-siRNA-CTX *in vitro* gene silencing in BT474-Gluc BMBC cell lines (Luciferase siRNA knockdown) (Months 1-12).

A pilot experiment was performed to compare GFP transgene silencing in an MMP-2 positive cell lines (C6/GFP+ and one MMP-2 negative MCF/GFP+ cell line were evaluated in this study (Figure 11). In this experiment cells where treated with nanoparticles at a concentration of 20 μg of Fe/ml for two hours after which time cells were rinsed and media was replaced and incubated for 48 hours prior to analysis. The results show that for the MMP-2 expressing cells we do see improved silencing through CTX modification. However, concerning is that silencing was observed in control MCF7 cells in both CTX modified and unmodified versions of nanoparticles. Future optimization of nanoparticles maybe necessary to improve the specificity of silencing

KEY RESEARCH ACCOMPLISHMENTS:

- Developed siRNA sequences to silence GFP, Luc, AHA1, and MENA/MENA-INV (Task 1a)
- Developed a synthesis scheme for preparing NPCP-siRNA-CTX and validated tumor cell specificity *in vitro* (Task 1b)
- Synthesized and validated NPCP-siRNA-CTX *in vitro* gene silencing in cancer cell lines (Task 1c)

PUBLICATIONS, ABSTRACTS, AND PRESENTATIONS:

Peer-Reviewed Publications:

1. Kathryn A. Whitehead, Robert Dorkin, Arturo Vegas, Philip Chang, Omid Veiseh, Jonathan Matthews, Owen Fenton, Yunlong Zhang, Karsten Olejnik, Delai Chen, Scott Barros, Boris Klebanov, Tatiana Novobrantseva, Robert Langer, and Daniel Anderson, Degradable Lipid-like Nanoparticles with Predictable In Vivo siRNA Delivery Activity, Nature Communications, 5(4277); 1-10 (2014)

2. Ahmed A. Eltoukhy, Delai Chen, Omid Veiseh, Jeisa Pelet, Hao Yin, Yizhou Dong, and Daniel Anderson, Nucleic Acid Conjugation Enables Efficient Intracellular Protein Delivery by Lipid-Based Nanoparticles, Biomaterials, 35(24); 6454-61 (2014)

3. Yizhou Dong, Ahmed A. Eltoukhy, Christopher Alabi, Omar Khan, Omid Veiseh, Robert Dorkin, Sasilada Sirirungruang, Hao Yin, Benjamin Tang, Jeisa M. Pelet, Delai Chen, Zhen Gu, Yuan Xue, Robert Langer, Daniel G. Anderson, Lipid-like nanomaterials for simultaneous gene expression and silencing in vivo, Advanced Healthcare Materials, In Press (2014)

Conferences Workshops and Presentations

Oral Presentations:

1. Robert S. Langer Seminar Series, David H. Koch Institute for Integrative Cancer Research, Cambridge, MA (March 2014)

2. Nanostring User Meeting, Broad Institute of MIT and Harvard, Cambridge, MA (June, 2014)

3. 12th Annual US-Japan Symposium on Drug Delivery Systems, Lahaina, Maui, HI (December, 2013)

Poster presentations:

- Gordon Research Conference: Drug Carriers in Medicine and Biology, Waterville Valley, NH (August 2014)

INVENTIONS, PATENTS AND LICENSES: None

REPORTABLE OUTCOMES: None

OTHER ACHIEVEMENTS:

Awarded the 2013 Koch Institute Marlena Felter Bradford Research Travel Fellowship ($1,200 award)

CONCLUSION:

Through the first year of this research proposal we developed this nanovector, and devised and optimized a synthesis approach, which produces uniform nanoparticles with high dispersity, magnetic relaxivity, functionality, and stability. The targeting capability of this magnetic nanovector was additionally evaluated in vitro using brain tumor cell lines that express the reporter gene AHA1 and proved effective in silencing AHA1 house keeping gene expression in breast cancer tumor cells. To further advance this project, this year our goal will be evaluate the therapeutic potential of the nanovector. We will first develop NPCP-siRNA-CTX nanovectors loaded with therapeutic siRNA sequenced designed to knockdown MENA/MENA-INV expression and monitor the delivering anti-MENA/MENA-INV siRNA to breast cancer cells in vitro and monitor its ability to induce cell kill. Next the nanovector will be evaluated in vivo in mouse models to monitor pharmacokinetics and optimize BBB permeability, and finally the therapeutic potential of the nanovector will be evaluated in vivo using brain metastatic breast cancer models. Upon completion of this project an optimized nanovector will be developed, which is detectable by MRI, capable of effectively delivering siRNA to target MB cells and down-regulating (or blocking) MENA/MENA-INV gene expression.

REFERENCES

1. J. S. Barnholtz-Sloan, A. E. Sloan, F. G. Davis, F. D. Vigneau, P. Lai, R. E. Sawaya, Incidence proportions of brain metastases in patients diagnosed (1973 to 2001) in

the Metropolitan Detroit Cancer Surveillance System. *J Clin Oncol* **22**, 2865-2872 (2004); published online EpubJul 15 (10.1200/JCO.2004.12.149).
2. L. J. Schouten, J. Rutten, H. A. Huveneers, A. Twijnstra, Incidence of brain metastases in a cohort of patients with carcinoma of the breast, colon, kidney, and lung and melanoma. *Cancer* **94**, 2698-2705 (2002); published online EpubMay 15 (
3. S. S. Lee, J. H. Ahn, M. K. Kim, S. J. Sym, G. Gong, S. D. Ahn, S. B. Kim, W. K. Kim, Brain metastases in breast cancer: prognostic factors and management. *Breast Cancer Res Treat* **111**, 523-530 (2008); published online EpubOct (10.1007/s10549-007-9806-2).
4. S. Lentzsch, P. Reichardt, F. Weber, V. Budach, B. Dorken, Brain metastases in breast cancer: prognostic factors and management. *Eur J Cancer* **35**, 580-585 (1999); published online EpubApr (
5. A. F. Eichler, J. S. Loeffler, Multidisciplinary management of brain metastases. *Oncologist* **12**, 884-898 (2007); published online EpubJul (10.1634/theoncologist.12-7-884).
6. F. Gertler, J. Condeelis, Metastasis: tumor cells becoming MENAcing. *Trends in cell biology* **21**, 81-90 (2011); published online EpubFeb (10.1016/j.tcb.2010.10.001).
7. A. Lambrechts, A. V. Kwiatkowski, L. M. Lanier, J. E. Bear, J. Vandekerckhove, C. Ampe, F. B. Gertler, cAMP-dependent protein kinase phosphorylation of EVL, a Mena/VASP relative, regulates its interaction with actin and SH3 domains. *J Biol Chem* **275**, 36143-36151 (2000); published online EpubNov 17 (10.1074/jbc.M006274200).
8. J. E. Bear, J. J. Loureiro, I. Libova, R. Fassler, J. Wehland, F. B. Gertler, Negative regulation of fibroblast motility by Ena/VASP proteins. *Cell* **101**, 717-728 (2000); published online EpubJun 23 (
9. M. Veiseh, P. Gabikian, S. B. Bahrami, O. Veiseh, M. Zhang, R. C. Hackman, A. C. Ravanpay, M. R. Stroud, Y. Kusuma, S. J. Hansen, D. Kwok, N. M. Munoz, R. W. Sze, W. M. Grady, N. M. Greenberg, R. G. Ellenbogen, J. M. Olson, Tumor paint: a chlorotoxin:Cy5.5 bioconjugate for intraoperative visualization of cancer foci. *Cancer Res* **67**, 6882-6888 (2007); published online EpubJul 15 (67/14/6882 [pii]
10.1158/0008-5472.CAN-06-3948).
10. O. Veiseh, C. Sun, C. Fang, N. Bhattarai, J. Gunn, F. Kievit, K. Du, B. Pullar, D. Lee, R. G. Ellenbogen, J. Olson, M. Zhang, Specific targeting of brain tumors with an optical/magnetic resonance imaging nanoprobe across the blood-brain barrier. *Cancer Res* **69**, 6200-6207 (2009); published online EpubAug 1 (0008-5472.CAN-09-1157 [pii]
10.1158/0008-5472.CAN-09-1157).
11. K. Kesavan, J. Ratliff, E. W. Johnson, W. Dahlberg, J. M. Asara, P. Misra, J. V. Frangioni, D. B. Jacoby, Annexin A2 is a molecular target for TM601, a peptide with tumor-targeting and anti-angiogenic effects. *J Biol Chem* **285**, 4366-4374 (2010); published online EpubFeb 12 (10.1074/jbc.M109.066092).

12. A. de Fougerolles, H. P. Vornlocher, J. Maraganore, J. Lieberman, Interfering with disease: a progress report on siRNA-based therapeutics. *Nat Rev Drug Discov* **6**, 443-453 (2007); published online EpubJun (10.1038/nrd2310).
13. S. Laurent, D. Forge, M. Port, A. Roch, C. Robic, L. V. Elst, R. N. Muller, Magnetic iron oxide nanoparticles: Synthesis, stabilization, vectorization, physicochemical characterizations, and biological applications. *Chemical Reviews* **108**, 2064-2110 (2008); published online EpubJun (10.1021/cr068445e).

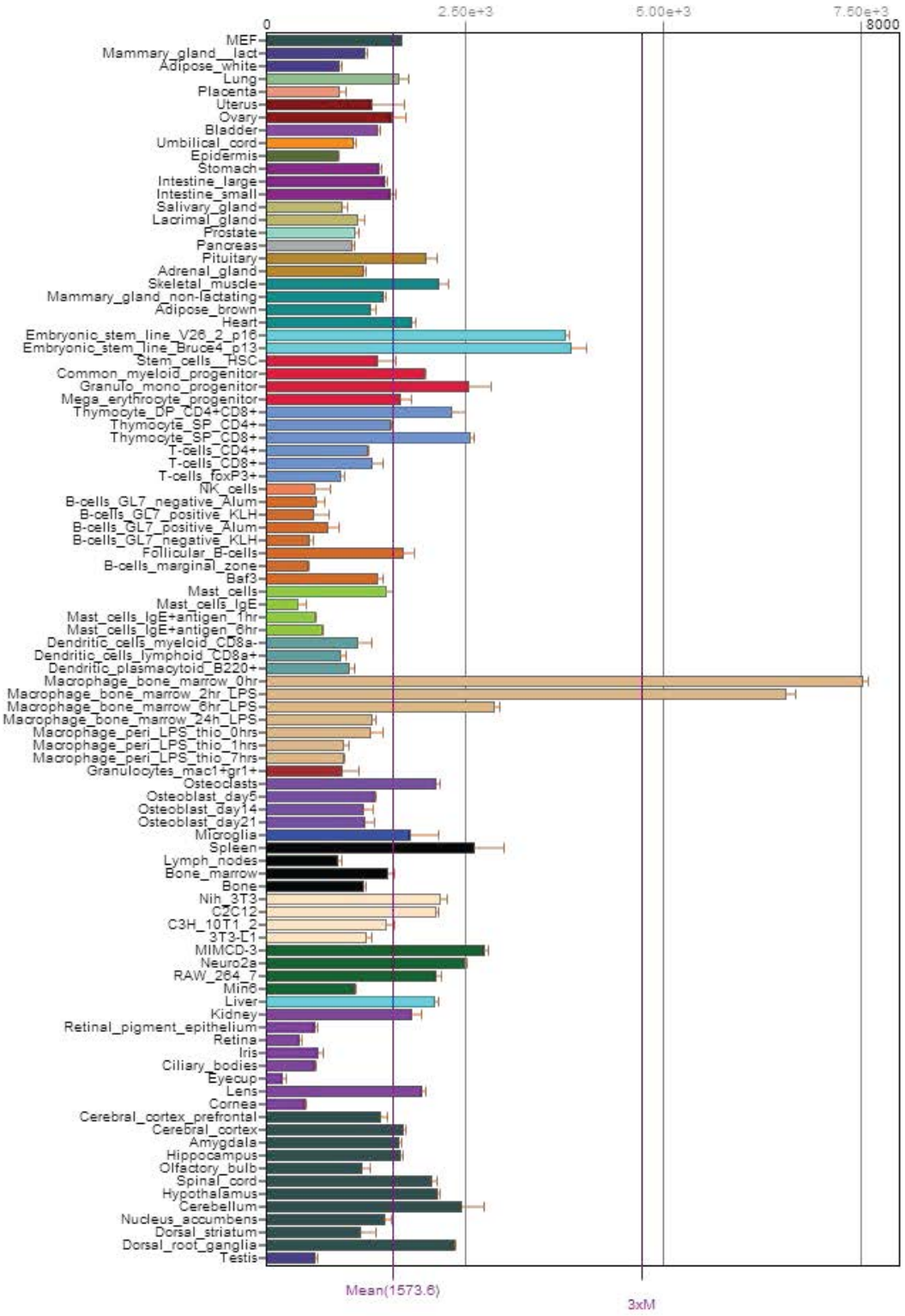
0
2.50e+3
5.00e+3
7.50e+3
8000
MEF
Mammary_gland__lact
Adipose_white
Lung
Placenta
Uterus
Ovary
Bladder
Umbilical_cord
Epidermis
Stomach
Intestine_large
Intestine_small
Salivary_gland
Lacrimal_gland
Prostate
Pancreas
Pituitary
Adrenal_gland
Skeletal_muscle
Mammary_gland_non-lactating
Adipose_brown
Heart
Embryonic_stem_line_V26_2_p16
Embryonic_stem_line_Bruce4_p13
Stem_cells__HSC
Common_myeloid_progenitor
Granulo_mono_progenitor
Mega_erythrocyte_progenitor
Thymocyte_DP_CD4+CD8+
Thymocyte_SP_CD4+
Thymocyte_SP_CD8+
T-cells_CD4+
T-cells_CD8+
T-cells_foxP3+
NK_cells
B-cells_GL7_negative_Alum
B-cells_GL7_positive_KLH
B-cells_GL7_positive_Alum
B-cells_GL7_negative_KLH
Follicular_B-cells
B-cells_marginal_zone
Baf3
Mast_cells
Mast_cells_IgE
Mast_cells_IgE+antigen_1hr
Mast_cells_IgE+antigen_6hr
Dendritic_cells_myeloid_CD8a-
Dendritic_cells_lymphoid_CD8a+
Dendritic_plasmacytoid_B220+
Macrophage_bone_marrow_0hr
Macrophage_bone_marrow_2hr_LPS
Macrophage_bone_marrow_6hr_LPS
Macrophage_bone_marrow_24h_LPS
Macrophage_peri_LPS_thio_0hrs
Macrophage_peri_LPS_thio_1hrs
Macrophage_peri_LPS_thio_7hrs
Granulocytes_mac1+gr1+
Osteoclasts
Osteoblast_day5
Osteoblast_day14
Osteoblast_day21
Microglia
Spleen
Lymph_nodes
Bone_marrow
Bone
Nih_3T3
C2C12
C3H_10T1_2
3T3-L1
MIMCD-3
Neuro2a
RAW_264_7
Min6
Liver
Kidney
Retinal_pigment_epithelium
Retina
Iris
Ciliary_bodies
Eyecup
Lens
Cornea
Cerebral_cortex_prefrontal
Cerebral_cortex
Amygdala
Hippocampus
Olfactory_bulb
Spinal_cord
Hypothalamus
Cerebellum
Nucleus_accumbens
Dorsal_striatum
Dorsal_root_ganglia
Testis
Mean(1573.6)
3xM

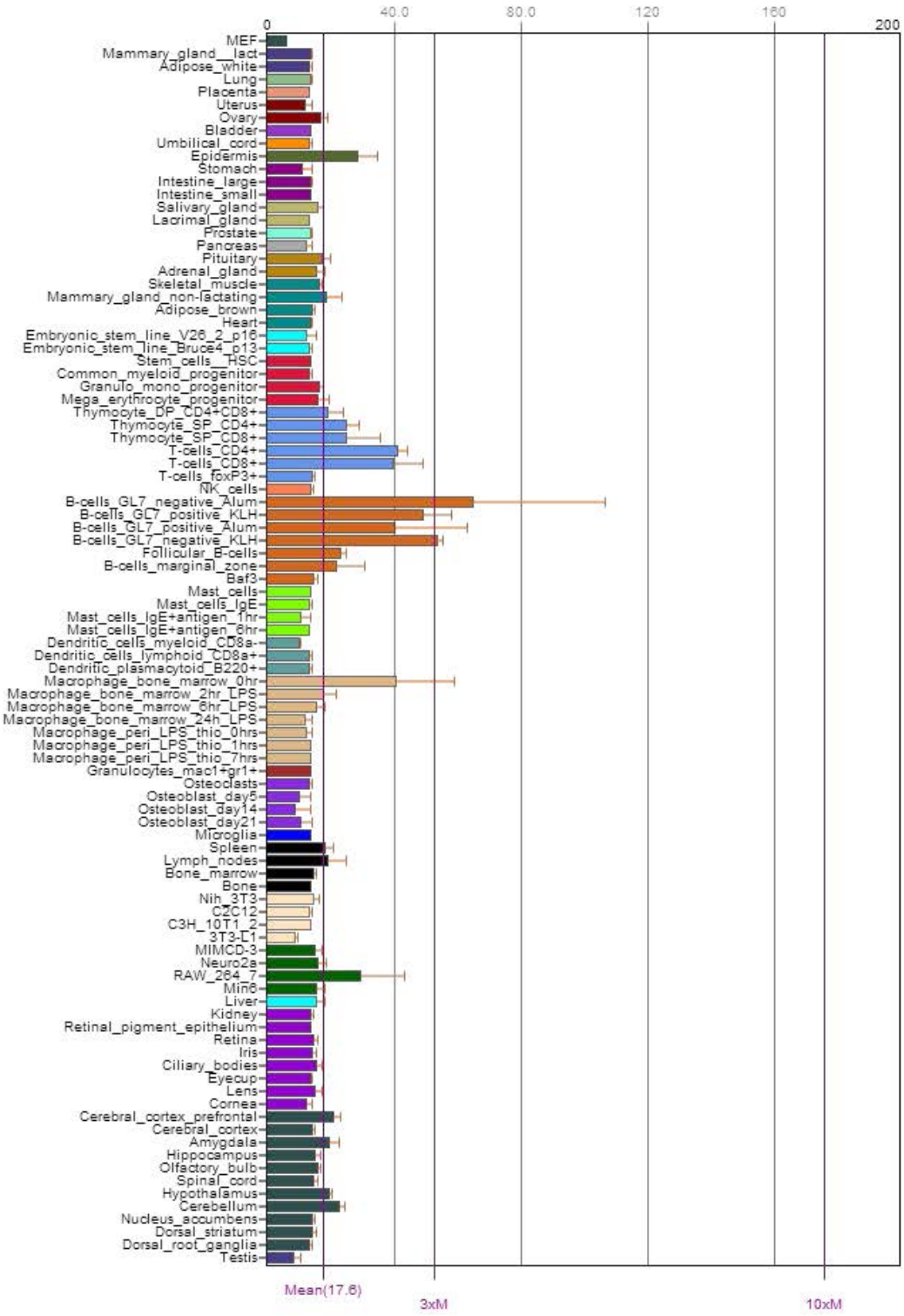

Figure 1. AHA1 expression in mouse cells and tissue

Table 1 Design of 6 siRNA sequences for silencing MENA and its invasive isoform MENA-INV

- 6 siRNAs
  - 3 siRNAs were selected to be x-reactive with INV4 and INV7 sequences (Ensembl exon IDs ENSE00001442739 and ENSE00001442738)
  - 3 siRNAs were selected to be x-reactive with as many as possible human and mouse ENAH transcripts
- Predicted to be specific in human and mouse
- No conserved miRNA seed regions (nucleotide positions 2-7) in both siRNA strands

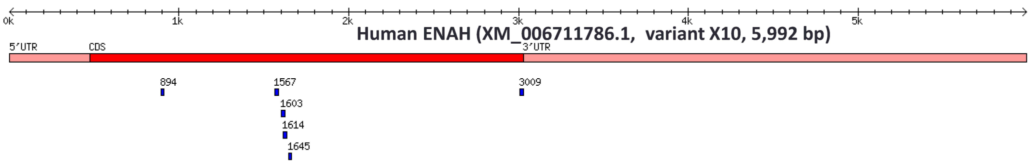

ID (position in XM_006711786.1)	INV target	core sense strand sequence (5´-3´)	core antisense strand sequence (5´-3´)
894	inv4	GCACUAAUUUGCGAUGUAU	AUACAUCGCAAAUUAGUGC
1567	inv7	GACACGUUUUGCAACAUCU	AGAUGUUGCAAAACGUGUC
1645	inv7	CAAAAACUCUCGACCUUCU	AGAAGGUCGAGAGUUUUUG
1603	-	GAAGACAAUCGCCCUUUAA	UUAAAGGGCGAUUGUCUUC
1614	-	CCCUUUAACUGGACUUGCA	UGCAAGUCCAGUUAAAGGG
3009	-	GUAAUUACAAUCACCACAA	UUGUGGUGAUUGUAAUUAC

cross- species homology — HUMAN — NCBI ResSeq

ID	NM_018212.4	NM_001008493.1	XM_005273182.1	XM_005273187.1	XM_005273188.1	XM_005273189.1	XM_006711786.1	XM_006711787.1	XM_006711788.1	XM_006711789.1	XM_006711790.1	XM_006711791.1	XM_006711792.1	XM_006711793.1	XM_006711794.1	XM_006711795.1	XM_006711796.1	XM_006711797.1
894	0	0	0	0	0	0	1	1	0	1	1	0	0	0	0	1	1	1
1567	0	0	1	0	0	0	1	1	1	1	1	1	1	1	1	0	0	0
1645	0	0	1	0	0	0	1	1	1	1	1	1	1	1	1	0	0	0
1603	1	1	1	1	1	1	1	1	1	1	1	1	1	1	1	1	1	1
1614	1	1	1	1	1	1	1	1	1	1	1	1	1	1	1	1	1	1
3009	1	1	1	1	1	1	1	1	1	1	1	1	1	1	1	1	1	1

HUMAN — Ensembl / exons

ID	ENST00000366844	ENST00000488523	ENST00000358675	ENST00000366843	ENST00000284563	ENST00000498108	ENST00000483952	ENST00000497899	ENST00000391874	ENSE00003567376	ENSE00001442739 INV4	ENSE00003485859	ENSE00003463753	ENSE00001442738 INV7	ENSE00001129400
894	0	0	0	0	1	0	0	0	0	0	1	0	0	0	0
1567	0	0	0	0	1	0	0	0	0	0	0	0	0	1	0
1645	0	0	0	0	1	0	0	0	0	0	0	0	0	1	0
1603	1	0	1	1	1	0	0	0	0						
1614	1	0	1	1	1	0	0	0	0						
3009	1	0	1	0	0	0	0	0	0						

MOUSE — NCBI RefSeq

ID	NM_008680.3	NM_010135.3	NM_001083120.2	NM_001083121.2	XM_006496643.1	XM_006496644.1	XM_006496645.1	XM_006496646.1	XM_006496647.1	XM_006496648.1	XM_006496649.1	XM_006496650.1	XM_006496651.1	XM_006496652.1
894	0	1	0	0	1	1	0	0	0	1	1	0	0	0
1567	1	1	1	0	1	1	1	1	1	1	1	0	0	0
1645	1	1	1	0	1	1	1	1	1	1	1	0	0	0
1603	1	1	1	1	1	1	1	1	1	1	1	1	1	1
1614	1	1	1	1	1	1	1	1	1	1	1	1	1	1
3009	1	1	1	1	0	0	0	0	0	0	0	0	0	0

MOUSE — Ensembl / exons

ID	ENSMUST00000078719	ENSMUST00000111030	ENSMUST00000177811	ENSMUST00000111024	ENSMUST00000111025	ENSMUSE00000336502	ENSMUSE00000446160 INV4	ENSMUSE00000446155	ENSMUSE00000446152	ENSMUSE00000370935 INV7	ENSMUSE00000461244
894	1	0	0	0	0	0	1	0	0	0	0
1567	1	1	1	1	0	0	0	0	0	1	0
1645	1	1	1	1	0	0	0	0	0	1	0
1603	1	1	1	1	1						
1614	1	1	1	1	1						
3009	1	1	1	1	1						

1 – perfect match with 19mer; 0 – at least 1 mismatch or missing target region

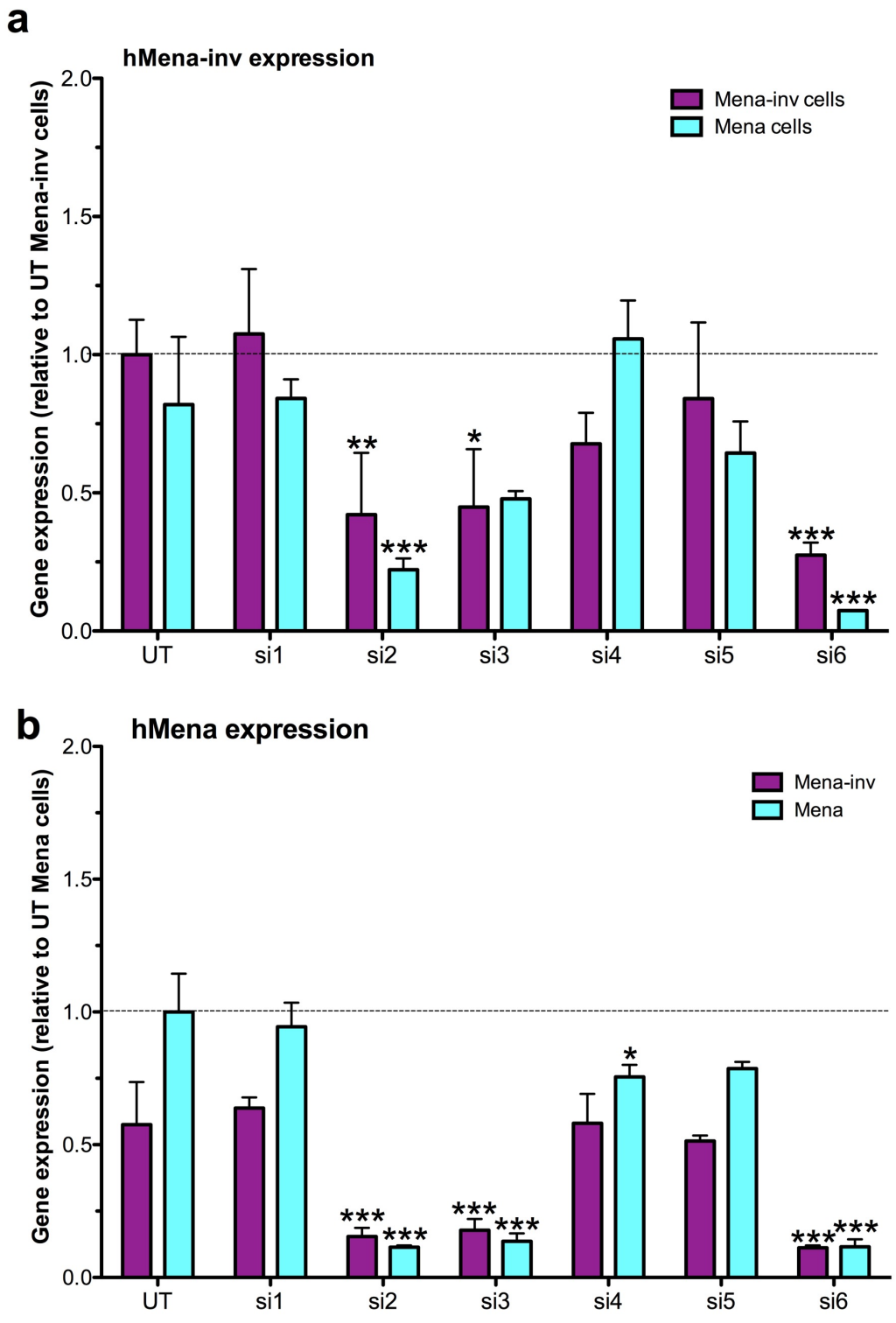

Figure 2. screening 5 different siRNA sequences to identify a sequence which is efficacious at silencing both MENA and its invasive isoform MENA-inv. qPCR analysis of

MDA-MB239 cells overexpressing MENA or MENA-INV treated with siRNA 1-6. These results suggest that siRNA 6 is most efficacious.

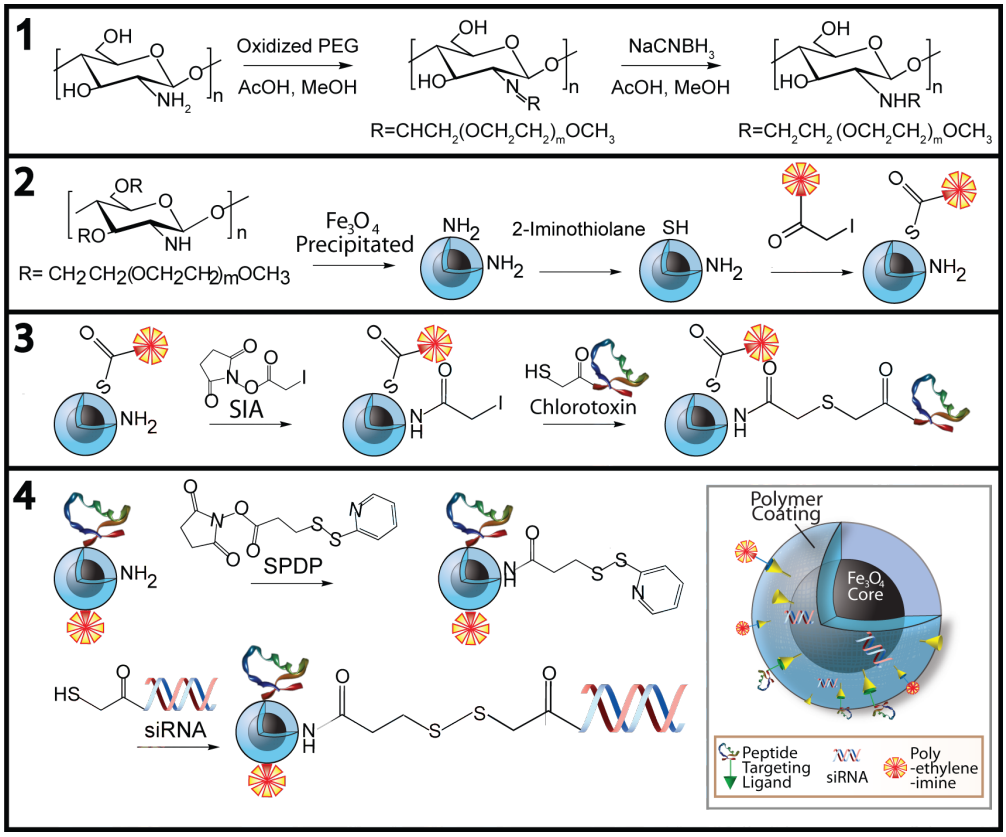

Figure 3: Schematic for the synthesis and chemical conjugation used for preparation of NPC-PEG-PEI-siRNA-CTX.

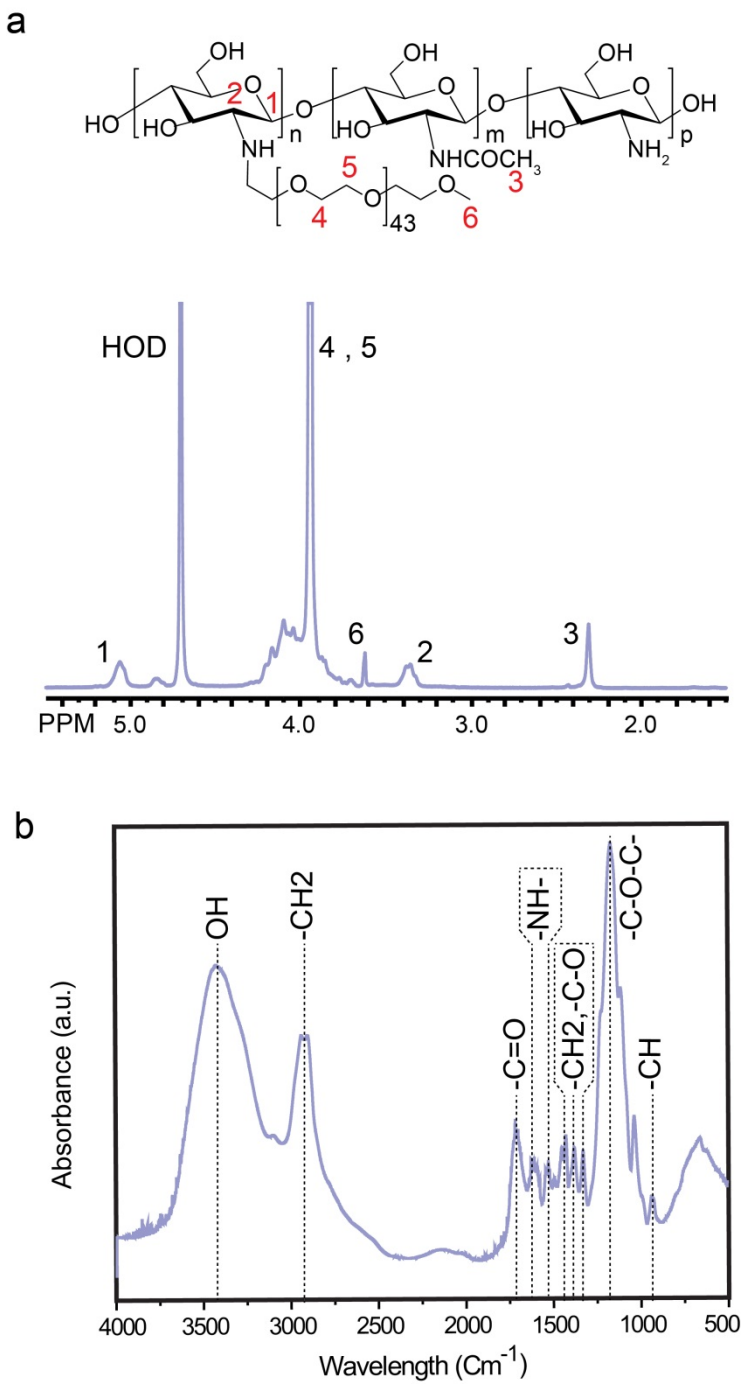

Figure 4. (a) ^{1}H NMR spectrum of the PEG-g-chitosan copolymer after removing of the unreacted PEG molecules, showing the incorporation of PEG onto chitosan backbone. The sample was analyzed in D_2O. (b) FTIR spectrum of the PEG-g-chitosan copolymer coating.

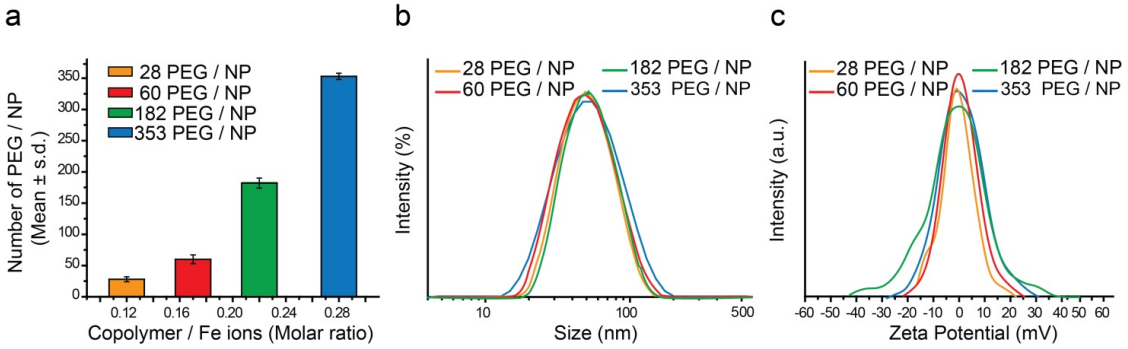

Figure 5. (a) Variation of the average number of PEG molecules per nanoparticle, hydrodynamic size (b) and zeta potential (c) of the nanoparticles with polymer/(Fe^{2+}+Fe^{3+}) ions molar ratio.

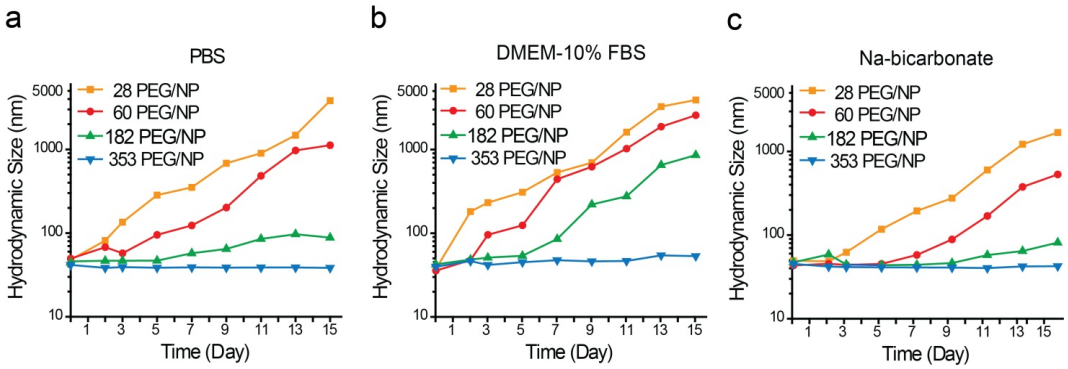

Figure 6. Long-term stability study of the nanoparticles coated with 28, 60, 182 and 353 PEG molecules per NP in (a) PBS, (b) sodium bicarbonate and (d) DMEM cell culture medium enriched with 10% FBS.

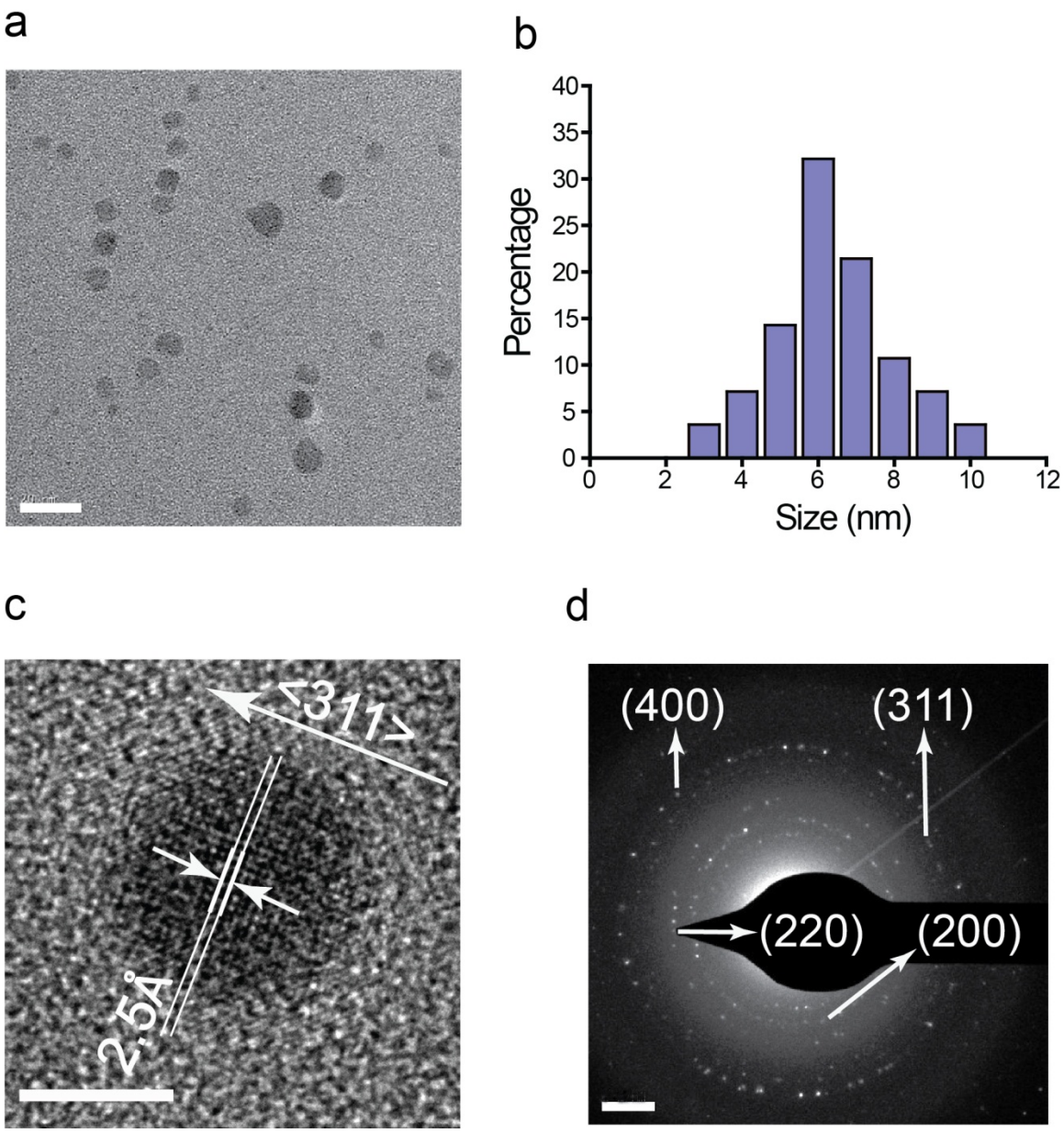

Figure 7. (a) Conventional TEM image (scale bar 20nm), (b) corresponding statistic size distribution, (c) high resolution TEM images (scale bar 5nm), and (d) selected area diffraction pattern (scale bar 2 1/nm) of the nanoparticles coated with about 353 PEG molecules per NP.

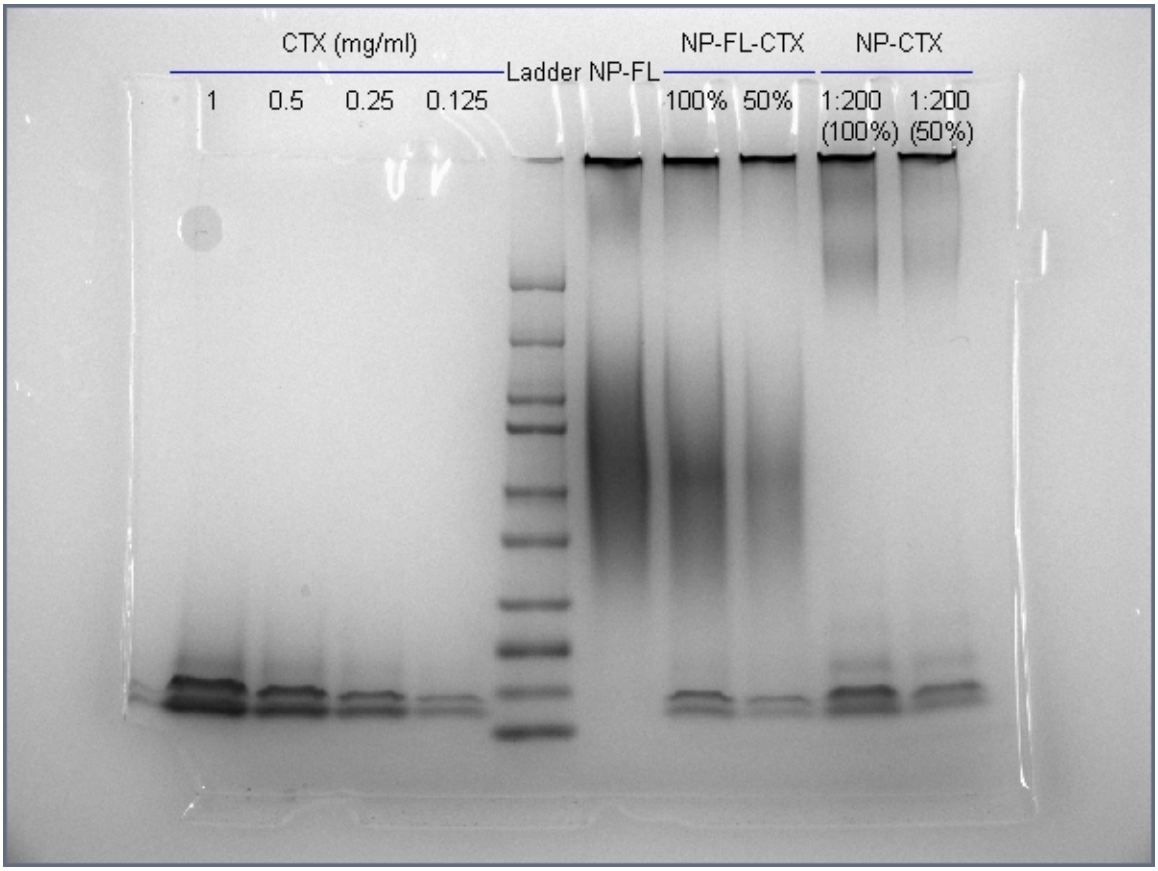

Figure 8: Gel electrophoresis assay evaluating CTX attachement to NPCP. Based on quantitation results it appears there was about a 75% CTX attachment efficiency.

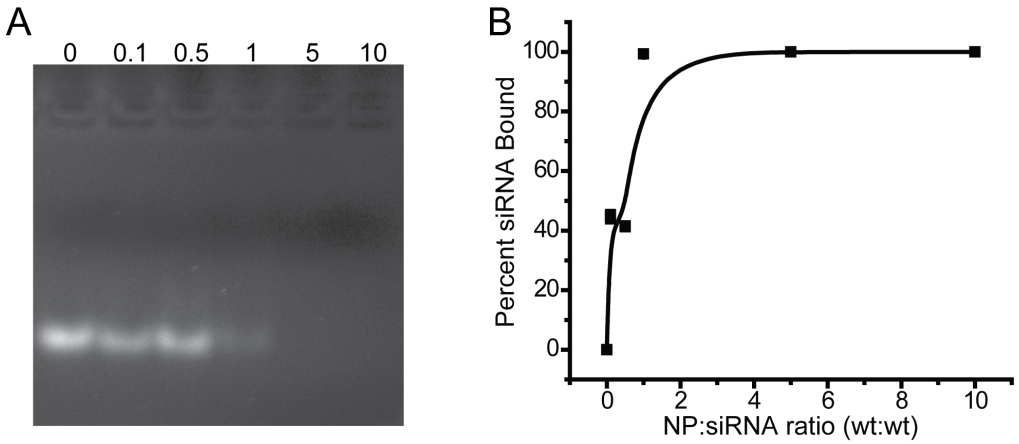

Figure 9. Characterization of siRNA binding by NPs. A) Image of Gel loaded from retardations assay study, the numbers above gel indicate the NP:siRNA ratio for sample loaded in each well. B) Quantification of bound siRNA.

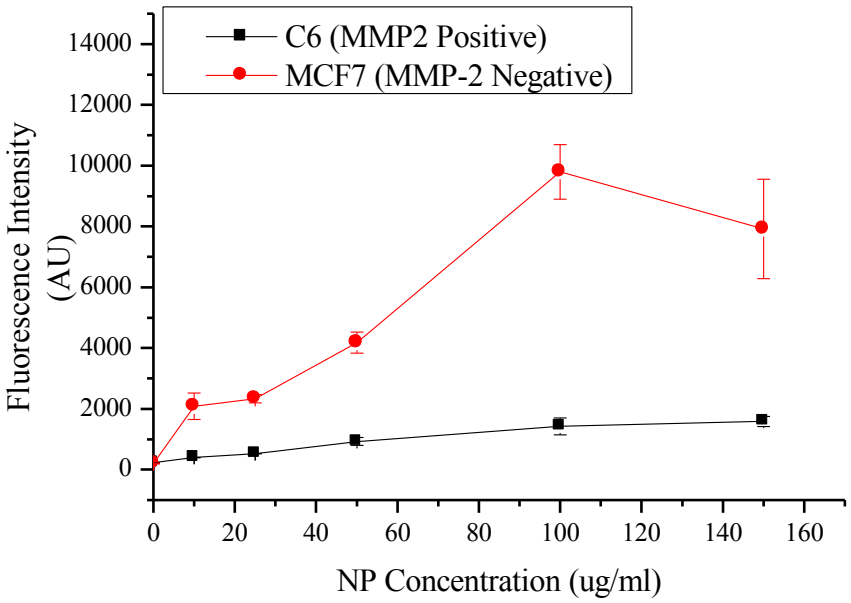

Figure 10: Comparative cell internalization of NPCP-Af-647-CTX nanoparticles by MMP-2 positive C6/GFP+ versus MMP-2 negative MCF-7 cells.

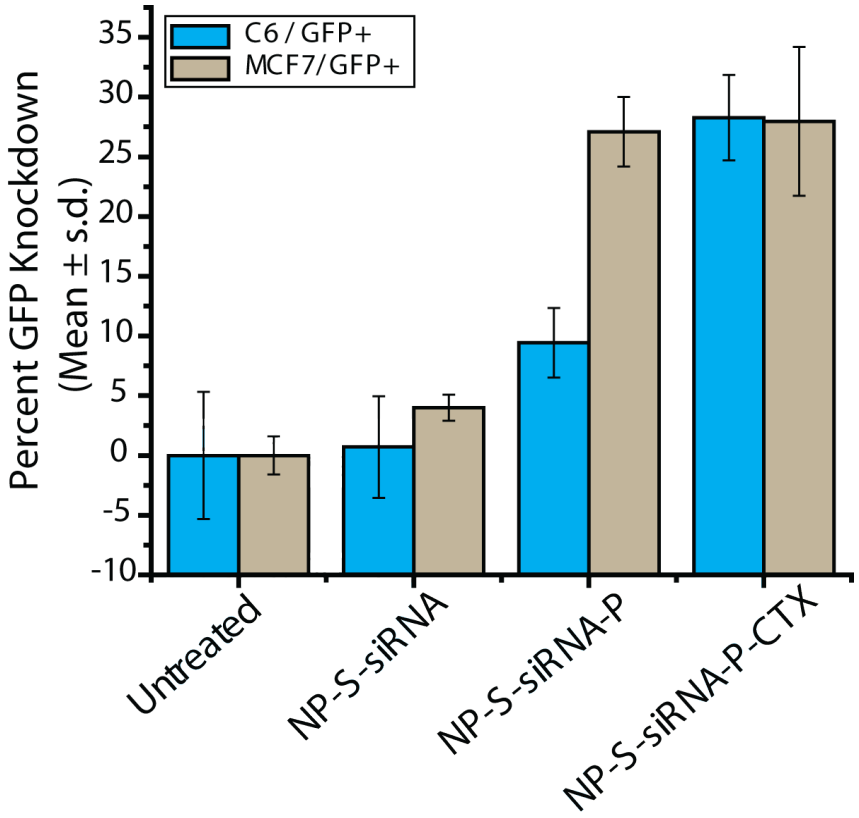

Figure 11: Flow cytometry analysis of cell untreated cells and post treatment with NP-S-siRNA, NP-S-siRNA-P, and NP-S-siRNA-P-CTX. In this study C6 cells are MMP-2 expressing and MCF7 cells are controls that do not express MMP2. The data is expressed in terms of percent knockdown in GFP expression.